

# Low Thermal Expansion of Layered Electrides Predicted by Density-Functional Theory

Adrian F. Rumson<sup>1</sup> and Erin R. Johnson<sup>1, a)</sup>

*Department of Chemistry, Dalhousie University, 6274 Coburg Rd, Halifax, Nova Scotia, B3H 4R2, Canada*

(Dated: 11 October 2023)

Layered electrides are a unique class of materials with anionic electrons bound in interstitial regions between thin, positively charged atomic layers. While density-functional theory is the tool of choice for computational study of electrides, there has to date been no systematic comparison of density functionals or dispersion corrections for their accurate simulation. There has also been no research into the thermomechanical properties of layered electrides, with computational predictions considering only static lattices. In this work, we investigate the thermomechanical properties of five layered electrides using density-functional theory to evaluate the magnitude of thermal effects on their lattice constant and cell volumes. We also assess the accuracy of five popular dispersion corrections with both planewave and numerical atomic orbital calculations.

## I. INTRODUCTION

Electrides are a class of solid-state ionic materials in which the anions are electrons localized within interstitial regions of the crystal lattice. These materials are of interest due to their unusual chemical properties and facile electron mobility. They have been shown to act as powerful and selective reducing agents,<sup>1,2</sup> and promise a role in the catalytic splitting of CO<sub>2</sub><sup>3</sup> and N<sub>2</sub>.<sup>4</sup> By exploiting their physical properties, they hold the potential to enable new technologies, such as Ohmic contacts with monolayer transition metal dichalcogenide semiconductors,<sup>5,6</sup> and advance existing ones, such as organic light-emitting diodes<sup>7</sup> and superconductors.<sup>8</sup>

The first reported electride was Cs<sup>+</sup>(18-crown-6)<sub>2</sub>e<sup>-</sup>, which is a organic sandwich complex of Cs<sup>+</sup> with electron-rich crown ether ligands that was first synthesised and characterized by Dye and coworkers in the 1980s.<sup>9,10</sup> The Dye group later reported a variety of analogous organic electrides based on various alkali metal cations complexed with either crown ether or cryptand ligands.<sup>11-14</sup> The first inorganic electride, [Ca<sub>24</sub>Al<sub>28</sub>O<sub>64</sub>]<sup>4+</sup>(4e<sup>-</sup>), was synthesized by the Hosono group<sup>15</sup> in 2003, opening the door to other possible electride stoichiometries.

Following the synthesis of [Ca<sub>24</sub>Al<sub>28</sub>O<sub>64</sub>]<sup>4+</sup>(4e<sup>-</sup>), a variety of other inorganic electride structures were identified.<sup>16</sup> Of particular interest is Ca<sub>2</sub>N, which was shown to be a layered electride in 2013.<sup>17</sup> This material has a hexagonal layered structure belonging to the  $R\bar{3}m$  space group. Each layer is a positively charged ionic slab, and the loosely bound anionic electrons exist within the interstitial regions between them (see Figure 1(a)). In 2016, it was experimentally demonstrated that Ca<sub>2</sub>N can be exfoliated,<sup>18</sup> and a number of theoretical studies have examined both the exfoliation energy of the bulk electride and the electronic structure of monolayer Ca<sub>2</sub>N, termed an electrene.<sup>5,19-24</sup>

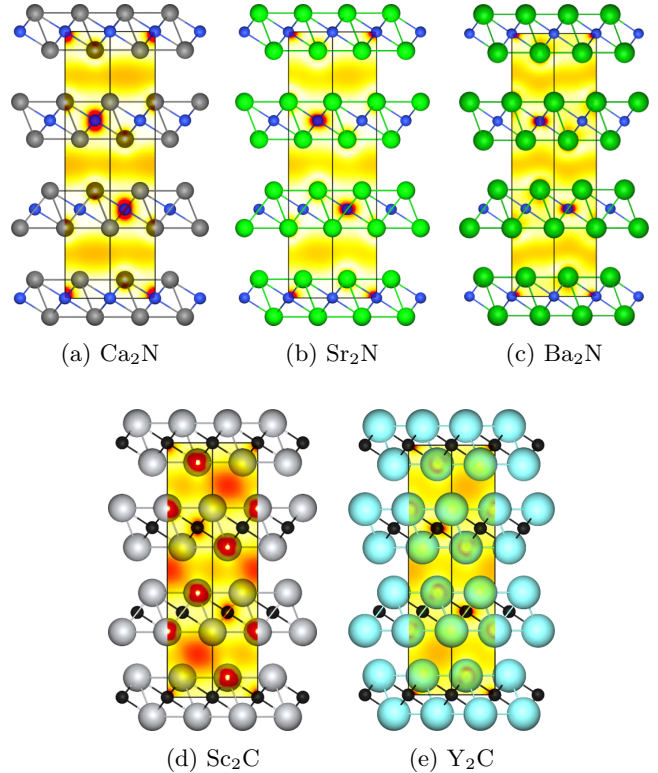


FIG. 1: Structures of the five layered electrides considered in this work, superimposed with the integrated local density of states (ILDOS, within 0.5 eV of the Fermi level) to visualize the interstitial electrons.

The white-yellow-orange-red colour scale spans an isodensity range of 0-0.005 a.u. for the nitrides and 0-0.01 a.u. for the carbides. Calculations correspond to B86bPBE-XDM/PAW (see Section II for details).

Hosono and coworkers<sup>17</sup> also proposed that other alkaline earth (AE) nitrides possessing a stoichiometric formula of [AE<sub>2</sub>N]<sup>+</sup>e<sup>-</sup>, and exhibiting a layered structure similar to that of Ca<sub>2</sub>N, could be synthesized. Several computational studies have since searched for other stable layered electrides,<sup>25-28</sup> resulting in the identifi-

<sup>a)</sup>Electronic mail: erin.johnson@dal.ca

cation and experimental characterization of several 2D-electrides with the  $[\text{AE}_2\text{N}]^+e^-$  stoichiometry, including  $\text{Sr}_2\text{N}$  and  $\text{Ba}_2\text{N}$ .<sup>25,29</sup> Additionally, other materials displaying more exotic chemical compositions, but similar  $R\bar{3}m$  layered structures, have also been found to be electrides. Layered  $[\text{M}_2\text{C}]^{2+}(2e^-)$  structures have been determined for a variety of metallic elements with a 3+ oxidation state,<sup>21</sup> including  $\text{Y}_2\text{C}$ ,<sup>30</sup>  $\text{Sc}_2\text{C}$ ,<sup>31</sup>  $\text{Gd}_2\text{C}$ ,<sup>32</sup>  $\text{Tb}_2\text{C}$ ,<sup>33</sup>  $\text{Dy}_2\text{C}$ ,<sup>34</sup> and  $\text{Ho}_2\text{C}$ .<sup>35</sup>  $\text{Sc}_2\text{C}$  is an especially interesting case; unlike all other inorganic electrides, which are metallic in nature, it has been characterized as a semiconductor.<sup>31,36</sup> While this material is structurally analogous to the other layered electride materials, it presents an indirect band gap.<sup>36</sup> The opening of a band gap has been proposed to be due to the greater electronegativity of scandium compared to the other known electride-forming metals, lowering the energy of the unoccupied scandium orbitals and allowing them to hybridize with the occupied interstitial electride states.

The majority of electride studies have employed density-functional theory (DFT), the tool of choice for computational materials science, to characterize their electronic structure. However, there has yet to be a systematic assessment of the accuracy of density functionals for structural and energetic properties of layered electride materials. Accurate modelling of London dispersion is especially important for layered materials, and this physics must be added to most common DFT methods through the use of a dispersion correction. Several studies have demonstrated the sensitivity of DFT predictions of both out-of-plane lattice constants and exfoliation energies of layered transition-metal dichalcogenides to the choice of dispersion correction.<sup>37–39</sup> While the majority of the interlayer binding in layered electrides is due to electrostatics, dispersion still plays a significant role<sup>22</sup> and, as they also contain metals, it is likely that the predicted properties of these materials will be fairly sensitive to the choice of dispersion correction. It is, however, unclear if the differences between dispersion methods will be reduced or magnified for layered electrides given their unusual electronic structure.

Further, few papers have explored the thermal and mechanical properties of electrides, and those that have focused on  $[\text{Ca}_{24}\text{Al}_{28}\text{O}_{64}]^{4+}(4e^-)$ .<sup>40–42</sup> This leaves a gap in the literature surrounding layered electrides, which promise unique thermomechanical (and thermoelectric) characteristics thanks to the layers of interstitial electron density. To our knowledge, no research – experimental or computational – has yet explored the thermal expansion of layered electrides.

In this work, DFT calculations are performed for the five layered electride materials shown in Figure 1, the crystal structures of which have been well characterized experimentally.<sup>30,31,43</sup> Three of the five are alkaline earth metal nitrides ( $\text{Ca}_2\text{N}$ ,  $\text{Sr}_2\text{N}$ , and  $\text{Ba}_2\text{N}$ ),<sup>43</sup> while the remaining two are Group 3 transition-metal carbides ( $\text{Sc}_2\text{C}$ <sup>31</sup> and  $\text{Y}_2\text{C}$ <sup>30</sup>). Although there are also several known lanthanide metal carbide electrides, lanthanide

chemistry presents additional challenges for DFT and, thus, these materials are not included in this work. We aim to assess the accuracy of four popular dispersion corrections – TS,<sup>44</sup> MBD-NL,<sup>45</sup> D3,<sup>46,47</sup> and XDM<sup>48–50</sup> – for predicting the out-of-plane lattice constants and unit-cell volumes of the five layered electrides. Additionally, through use of both the Debye model and the quasi-harmonic approximation, we provide the first evaluation of their coefficients of thermal expansion.

## II. THEORY AND COMPUTATIONAL METHODS

This research employed generalized gradient approximation (GGA) density functionals paired with various post-self-consistent dispersion corrections. The dispersion corrections selected are the exchange-hole dipole moment (XDM)<sup>48–50</sup> model, the Tkachenko-Scheffler (TS)<sup>44</sup> model, and the ‘non-local’ variant of many-body dispersion (MBD-NL),<sup>45</sup> as well as Grimme’s 3rd-generation dispersion correction with both zero damping (D3)<sup>46</sup> and Becke-Johnson<sup>51</sup> damping (D3BJ).<sup>47</sup> All dispersion methods were paired with the PBE<sup>52</sup> functional since this is the recommended GGA to pair with TS and MBD-NL, and damping parameters are readily available for the other dispersion corrections due to the widespread popularity of PBE in the solid-state DFT community. Additional XDM calculations were performed with the B86bPBE functional,<sup>52,53</sup> as this is the recommended GGA to pair with XDM and it has been used in previous studies of layered electrides.<sup>5,22</sup>

Calculations were performed using two different electronic structure codes depending on the availability of the dispersion corrections. These are the Fritz-Haber institute *ab initio* materials simulations (FHI-aims) package<sup>54</sup> for XDM, TS, and MBD-NL, and Quantum ESPRESSO (QE)<sup>55</sup> for XDM, D3, and D3BJ. We note that the distribution version of QE had incorrectly entered the  $\langle r^4 \rangle / \langle r^2 \rangle$  parameter value used in the D3 and D3BJ dispersion methods for barium (viz. 0.15679528 a.u. instead of 10.15679528 a.u.), which was corrected for all calculations performed here.

The fundamental difference between FHIaims and QE is one of basis sets. QE is a planewave code, whereas FHIaims uses numerical atom centered orbitals (NAOs) of finite extent, which leads to near linear scaling for large systems. Planewaves basis sets are inherently capable of reliably modeling the interstitial electride states since these functions are independent of nuclear positions. However, the use of NAOs may be problematic for electrides as they involve electrons that are not localized about atomic centers. In the limit of a complete NAO basis set, even interstitial electrons can be accurately described, although this may require such a large number of functions as to be impractical depending on the relative distance between the interstitial electrons and atomic centres. Conventional wisdom is to include additional ba-

sis functions centered on ghost atoms (i.e. sites with no nuclear charge) when performing calculations with atom-centered basis sets on solvated electrons,<sup>56–59</sup> which possess localized electrons within solvent cavities. As such, this work will also serve to assess the accuracy of the relatively small and highly efficient NAO basis sets provided with FHI-aims for electrides.

With both programs, a  $10 \times 10 \times 4$   $\mathbf{k}$ -point mesh was used for calculations on all electrides, except for  $\text{Ba}_2\text{N}$ , where a  $10 \times 10 \times 3$   $\mathbf{k}$ -point mesh was used due to its longer  $c$  lattice parameter. Calculations on single monolayers of each electride were also performed to evaluate the exfoliation energies; these calculations used cell lengths of 40 Å in the  $c$  lattice direction to ensure sufficient vacuum spacing between the reference cell and its periodic images. For the QE calculations, projector augmented-wave (PAW) pseudopotentials were generated from the `ld1.x` code.<sup>60</sup> Converged plane-wave cutoffs of 160 and 1600 Ry were used for the kinetic energy and electron density, respectively, except for  $\text{Sc}_2\text{C}$ , where values of 120 and 1200 Ry were used. This choice was based on our previous work<sup>24</sup> for  $\text{Ca}_2\text{N}$ ,  $\text{Sr}_2\text{N}$ , and  $\text{Ba}_2\text{N}$ , and on convergence testing for  $\text{Y}_2\text{C}$  and  $\text{Sc}_2\text{C}$ . Methfessel-Paxton<sup>61</sup> smearing was used for most cases, the exceptions being  $\text{Y}_2\text{C}$  with PBE-XDM, PBE-D3, and PBE-D3BJ,  $\text{Ca}_2\text{N}$  with B86bPBE-XDM, and  $\text{Ba}_2\text{N}$  with B86bPBE-XDM, which used cold smearing<sup>62</sup> for improved convergence. The smearing parameters were set to 0.001 Ry or 0.01 Ry, except for the case of  $\text{Sc}_2\text{C}$  with B86bPBE-XDM, where a value of 0.05 Ry was used to aid convergence. The FHI-aims calculations used the ‘tier1’ basis functions comprising the ‘light’ basis set provided in the FHI-aims species defaults, along with the integration grids specified in the ‘tight’ species defaults.<sup>50</sup> Scalar relativistic effects were accounted for through the use of pseudopotentials with QE, and with the `relativistic atomic_zora scalar` keyword with FHIaims.<sup>54</sup>

A variable-cell relaxation was performed for each bulk electride at a sequence of pressures,  $P$ , both positive and negative. A typical range was  $-40 \leq P \leq 40$  kbar in increments of 5 kbar, although some combinations of materials and functionals required additional calculations at more negative or positive pressures due to neglect of stress-tensor contributions from changes in the dispersion coefficients with XDM (and MBD-NL).<sup>63</sup> These calculations produced a parabolic volume-energy equation of state curve,  $E_{\text{el}}(V)$ , from which static thermodynamic properties could be evaluated using the `gibbs2` software package.<sup>64</sup>

In order to model thermodynamic properties at finite temperatures, a vibrational Helmholtz free-energy correction,  $F_{\text{vib}}(V, T)$ , must be added to the DFT electronic energies,  $E_{\text{el}}(V)$ . The Gibbs energy at volume,  $V$ , and temperature,  $T$ , is then

$$G(V, T) = F(V, T) = E_{\text{el}}(V) + F_{\text{vib}}(V, T). \quad (1)$$

The thermal free-energy correction, expressed in atomic

units, is

$$F_{\text{vib}} = \int_0^\infty \left[ \frac{\omega}{2} + k_{\text{B}}T \ln \left( 1 - e^{-\omega/k_{\text{B}}T} \right) \right] g(\omega) d\omega, \quad (2)$$

where  $\omega$  is the vibrational frequency,  $g(\omega)$  is the phonon density of states, and  $k_{\text{B}}$  is Boltzmann’s constant.

The phonon density of states can be conveniently estimated using only the static equation of state via the Debye approximation, implemented in `gibbs2`.<sup>64</sup> Within the Debye approximation, the phonon density of states is defined in terms of the Debye frequency,  $\omega_{\text{D}}$ ,

$$g_{\text{D}}(\omega) = \begin{cases} \frac{9n\omega^2}{\omega_{\text{D}}^3} & \text{if } \omega < \omega_{\text{D}} \\ 0 & \text{if } \omega \geq \omega_{\text{D}} \end{cases}, \quad (3)$$

where  $n$  is the number of atoms in the unit cell. The Debye frequency is, in turn, given in terms of the Debye temperature,  $\Theta_{\text{D}}$ ,

$$\omega_{\text{D}} = k_{\text{B}}\Theta_{\text{D}}, \quad (4)$$

which can be computed from the static lattice parameters and bulk modulus. Expressing  $F_{\text{vib}}$  in terms of the Debye temperature yields<sup>64</sup>

$$F_{\text{vib}} = \frac{9}{8}nk_{\text{B}}\Theta_{\text{D}} + 3nk_{\text{B}}T \ln \left( 1 - e^{-\Theta_{\text{D}}/T} \right) - nk_{\text{B}}T \left( \frac{3T^3}{\Theta_{\text{D}}^3} \int_0^{\Theta_{\text{D}}/T} \frac{t^3 e^{-t}}{1 - e^{-t}} dt \right). \quad (5)$$

Armed with an approximation to the vibrational Helmholtz free energy, other thermodynamic parameters are easily computed. The parameters of interest to this work were the thermally-expanded cell volumes and  $c$  lattice parameters, as well as the coefficients of thermal expansion (CTE),

$$\alpha = \frac{1}{V} \left( \frac{\partial V}{\partial T} \right)_P. \quad (6)$$

Finally, to confirm the accuracy of the Debye model, comparison was made to analogous calculations using the full quasi-harmonic approximation (QHA). Here, calculations were performed with `phonopy`<sup>65</sup> to compute the phonon frequencies and density of states using a  $2 \times 2 \times 1$   $\mathbf{q}$ -point grid. Due to the computational expense of such phonon calculations, only the QE implementation of the B86bPBE-XDM method was considered. The thermal free-energy correction was then evaluated from Equation 2 by integrating the phonon density of states at each volume, also using `gibbs2`.<sup>64</sup>

### III. RESULTS AND DISCUSSION

#### A. Electronic structure

Figure 1 shows the structures of the five layered electrides that comprise our data set. The figure also shows

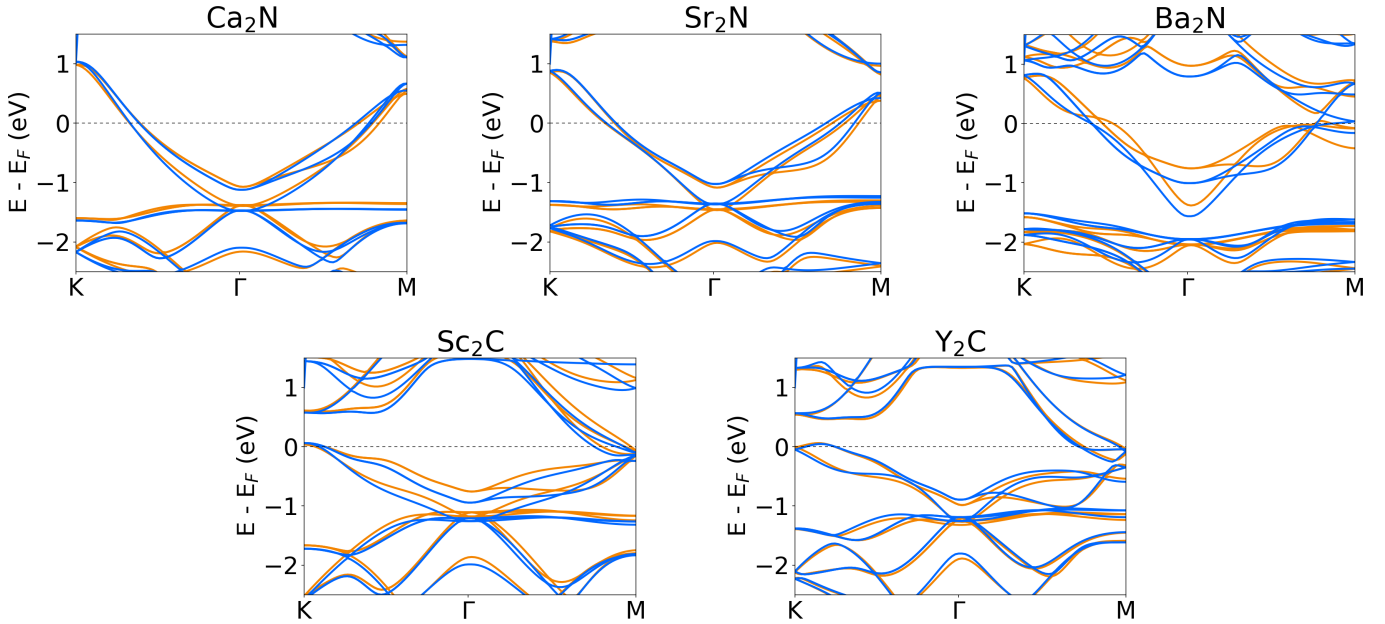


FIG. 2: Band structures of the five electrides computed with B86bPBE-XDM using both PAW (orange) and NAO (blue) approaches, at their respective optimized geometries.

the interstitial electron density through superimposing the structures with a heat map of the computed ILDOS for an energy range of  $-0.5 \text{ eV} \leq E \leq E_{\text{Fermi}}$ . This energy range was chosen based on examination of the computed band structures in Figure 2, which show clear electride bands crossing the Fermi level and with minima at  $\Gamma$  for each material.

An important consideration in this work is whether the highly efficient ‘light’ NAO basis sets are capable of accurately modeling electrides. With plane waves, the basis set is clearly capable of stabilizing electron density in the interstitial regions. However, it is unclear if the atom-centered NAOs used in FHI-aims are diffuse enough to do so without modification. To assess the ability of the ‘light’ NAO basis to model electride states, Figure 2 compares the computed band structures with planewave and NAO calculations. Both bases are found to give quite similar results, indicating that the light NAO basis is capable of predicting electride states, despite having no functions centered on ghost atoms in the interstitial regions.

Although  $\text{Sc}_2\text{C}$  has been characterized as a semiconductor,<sup>31</sup> calculations using both FHI-aims and QE display a conduction band that crosses below the Fermi level at  $M$ , as shown in Figure 2(d). This is explained by choice of functional, since McRae *et al.* employed the HSE06<sup>66</sup> hybrid functional instead of the B86bPBE GGA used here; GGAs are well known to predict metalization of small-gap semiconductors.<sup>67–69</sup> Thus, we also performed single-point calculations with FHI-aims using the HSE06 and PBE0<sup>70</sup> hybrid functionals, at the B86bPBE-XDM geometries, for both  $\text{Sc}_2\text{C}$  and  $\text{Y}_2\text{C}$ . The results confirmed the previous conclusion

of McRae *et al.*<sup>31</sup> that  $\text{Sc}_2\text{C}$  is a semiconductor, whereas  $\text{Y}_2\text{C}$  is metallic. The band structures obtained with both hybrid functionals are included in the Supplementary Material.

## B. Exfoliation energies

The computed exfoliation energies – the amount of energy required to isolate a monolayer from the bulk – of the five layered electrides are shown in Table I. It is immediately apparent upon inspection that these materials have very high exfoliation energies compared to dispersion-bound layered materials such as graphite ( $21 \pm 2 \text{ meV}/\text{\AA}^2$ )<sup>71</sup> or  $\text{MoS}_2$  ( $34 \pm 8 \text{ meV}/\text{\AA}^2$ ).<sup>72</sup> This is expected due to the ionic component to the interlayer binding, arising from the interactions between the positively charged atomic layers and the negatively charged electron-gas regions within the interstitial voids. The  $[\text{M}_2\text{C}]^{2+}(2e^-)$  transition metal carbides present exfoliation energies that are roughly twice as large as for the  $[\text{AE}_2\text{N}]^+(e^-)$  alkaline earth metal nitrides, which is also expected due to additional anionic electron per formula unit for the carbides. Finally,  $\text{Sc}_2\text{C}$  is predicted to have a greater exfoliation energy than  $\text{Y}_2\text{C}$  with all methods, likely due to the smaller atomic radii and increased hardness of the  $\text{Sc}^{3+}$  cations.

Comparing the XDM results between the PAW and NAO calculations, use of NAOs consistently results in stronger interlayer binding. This may be due to a combination of effects arising from limitations of the light NAO basis sets. First, for the bulk electrides, there may be some basis-set superposition error that would impart

TABLE I: Exfoliation energies (in meV/Å<sup>2</sup>) of the layered electrides computed with selected density functionals and dispersion corrections.

Method	Basis	Ca <sub>2</sub> N	Sr <sub>2</sub> N	Ba <sub>2</sub> N	Sc <sub>2</sub> C	Y <sub>2</sub> C
B86bPBE-XDM	PAW	97	80	71	193	147
PBE-XDM	PAW	69	55	59	173	120
PBE-D3	PAW	81	66	47	166	122
PBE-D3BJ	PAW	83	64	46	171	124
B86bPBE-XDM	NAO	111	105	112	209	168
PBE-XDM	NAO	103	100	115	204	163
PBE-MBD-NL	NAO	–	–	66	–	123
PBE-TS	NAO	157	141	173	254	182

greater stability relative to the exfoliated monolayers. Second, for the monolayers, the NAOs likely provide a poorer description of the diffuse surface states than with planewave basis sets due to their finite extent, resulting in destabilization of the monolayers relative to the bulk. Alternatively, the NAO basis sets can provide a more complete description of the dispersion coefficients, resulting in larger values for bulk metals than obtained with planewaves,<sup>73</sup> due to contributions from the core electrons that are missing when replaced by the PAW pseudopotentials.

Also of interest, there is a periodic trend in the B86bPBE-XDM/PAW exfoliation energies of the AE<sub>2</sub>N electrides, specifically a systematic decrease in exfoliation energy going down the alkaline earth metal group. This has also been observed from PAW calculations using the D3 and D3BJ dispersion corrections and can be explained by the smaller atomic radii for the lighter metals that should lead to stronger ionic bonding.<sup>24</sup> While this is countered by larger atoms being more polarizable, leading to stronger dispersion binding, the ionic effect still dominates the exfoliation energy trend in the PAW calculations. However, this periodic trend is not seen in the NAO data, with Ba<sub>2</sub>N instead presenting the highest exfoliation energy among the alkaline earth nitrides. This could be attributed to (i) larger basis-set incompleteness errors in the light NAO basis set for Ba relative to the other alkali metals; (ii) to a larger increase in the calculated dispersion coefficients of Ba with all-electron calculations due to its greater number of core electrons, leading to dominating van der Waals interactions; or (iii) some combination of the two. To test this, we performed additional calculations using the B86bPBE and PBE base density functionals without any dispersion correction (Supplementary Material). These results show that it is basis-set incompleteness that is primarily responsible for the altered trend, as the dispersion-uncorrected exfoliation energy for Ba<sub>2</sub>N is approximately equal to, or greater than, that of Sr<sub>2</sub>N with the NAO basis. Given the greater radial extent of Ba<sub>2</sub>N, it is expected that the ionic bonding in Ba<sub>2</sub>N should be weaker than for Sr<sub>2</sub>N, as seen in the PAW calculations.

Finally, given a consistent functional, we assess whether the choice of dispersion correction makes a sub-

stantial difference to the overall exfoliation energies. Table I shows that Grimme’s D3 and D3BJ corrections give similar results, implying that the choice of damping function makes little difference for these electrides. When paired with PBE, XDM also gives very similar results to the D3 methods for the carbides, although the results are less aligned for the nitrides, with XDM giving lower exfoliation energies for Ca<sub>2</sub>N and Sr<sub>2</sub>N, and a larger value for Ba<sub>2</sub>N. The reasons for the large change in exfoliation energies between B86bPBE and PBE with XDM only with the PAW, and not the NAO, basis are unclear. As seen previously for TMDCs, TS gives the largest exfoliation energies of the methods considered, which is likely due to using volume scaling in determination of the dispersion coefficients.<sup>44</sup> Conversely, where available, PBE-MBD-NL gives the lowest exfoliation energies of the NAO methods; however, the monolayer calculations failed for three of the electrenes due to a negative eigenvalue error in the MBD routine. Unfortunately, as there is no reference data from experiment or high-level theory, we cannot say which of the dispersion methods is the most accurate.

### C. Unit-cell volumes, lattice constants, and thermal expansion

Next we assess the performance of the various dispersion-corrected functionals for the unit-cell volumes and lattice constants, for which reference experimental data is available. For most solids, thermal expansion has a significant effect on the lattice constants and volumes so, to allow proper comparison with experiment, thermal effects must be included in the calculations. The computed cell volumes and out-of-plane (*c*-axis) lattice parameters, evaluated using the Debye approximation for all combinations of density functional and dispersion methods, are collected in Tables II and III, respectively.

The results show that, unlike for bulk metals,<sup>73</sup> the inclusion of thermal effects does not make a substantial difference in the computed cell volumes and lattice constants and actually results in a very slight increase in the mean absolute error (MAE) in most cases. In particular, the thermal expansion in the direction of the *c* lattice vector is very small – an unusual characteristic of both layered materials and most metals – which can be explained by the strong, ionic interlayer binding experienced due to the interactions between the cationic layers and anionic interstitial electrons. Interestingly, Y<sub>2</sub>C displays thermal contraction with some functionals, although a corresponding decrease in the *c*-parameter is not seen, indicating that the thermal contraction occurs in the (001) lattice plane.

Most functionals and dispersion corrections were found to provide fairly accurate predictions of the experimental cell volumes and lattice constants for the layered electrides. The exception is Ba<sub>2</sub>N, where PBE-XDM and PBE-TS underestimate the volume by ca. 30-40 Å<sup>3</sup> and

TABLE II: Static ( $V_0$ ) and thermally corrected ( $V_{\text{th}}$ ) volumes, in  $\text{\AA}^3$ , computed with selected density functionals and dispersion corrections using planewaves (top) and NAO basis sets (bottom). MAE: mean absolute error, relative to experiment.

Projector Augmented-Wave Method									
Electride	B86bPBE-XDM		PBE-XDM		PBE-D3		PBE-D3BJ		Experiment
	$V_0$	$V_{\text{th}}$	$V_0$	$V_{\text{th}}$	$V_0$	$V_{\text{th}}$	$V_0$	$V_{\text{th}}$	
Ca <sub>2</sub> N	203.2	204.1	200.2	201.4	210.4	211.2	206.9	208.0	198.03 <sup>43</sup>
Sr <sub>2</sub> N	248.6	249.9	239.2	240.2	260.9	262.0	257.4	259.0	240.12 <sup>43</sup>
Ba <sub>2</sub> N	287.9	288.9	260.4	260.9	312.1	314.2	307.7	309.8	304.53 <sup>43</sup>
Sc <sub>2</sub> C	154.4	155.7	154.6	155.8	155.2	155.7	153.8	154.2	159.01 <sup>31</sup>
Y <sub>2</sub> C	200.6	198.5	199.8	198.1	202.2	202.9	200.9	201.5	203.49 <sup>30</sup>
MAE	7.3	7.7	10.8	11.0	8.9	9.5	7.1	7.9	—

Numerical Atomic Orbitals									
Electride	B86bPBE-XDM		PBE-XDM		PBE-MBD-NL		PBE-TS		Experiment
	$V_0$	$V_{\text{th}}$	$V_0$	$V_{\text{th}}$	$V_0$	$V_{\text{th}}$	$V_0$	$V_{\text{th}}$	
Ca <sub>2</sub> N	201.3	202.8	203.0	204.2	208.5	209.5	188.7	189.0	198.03
Sr <sub>2</sub> N	245.3	246.2	245.1	246.5	254.3	255.6	244.1	245.3	240.12
Ba <sub>2</sub> N	271.8	273.5	265.1	267.3	279.5	281.0	264.5	265.7	304.53
Sc <sub>2</sub> C	153.0	153.0	154.6	154.9	154.0	154.4	148.1	148.5	159.01
Y <sub>2</sub> C	197.9	198.2	199.0	199.1	200.6	200.5	192.8	193.3	203.49
MAE	10.3	10.4	11.4	11.4	11.3	11.4	14.7	14.5	—

TABLE III: Static ( $c_0$ ) and thermally corrected ( $c_{\text{th}}$ ) out-of-plane lattice parameters, in  $\text{\AA}$ , computed with selected density functionals and dispersion corrections using planewaves (top) and NAO basis sets (bottom). MAE: mean absolute error, relative to experiment.

Projector Augmented-Wave Method									
Electride	B86bPBE-XDM		PBE-XDM		PBE-D3		PBE-D3BJ		Experiment
	$c_0$	$c_{\text{th}}$	$c_0$	$c_{\text{th}}$	$c_0$	$c_{\text{th}}$	$c_0$	$c_{\text{th}}$	
Ca <sub>2</sub> N	18.60	18.64	18.39	18.44	19.00	19.04	18.82	18.88	18.114 <sup>43</sup>
Sr <sub>2</sub> N	20.10	20.14	19.63	19.68	20.67	20.74	20.54	20.61	19.589 <sup>43</sup>
Ba <sub>2</sub> N	21.50	21.54	20.57	20.59	22.53	22.61	22.33	22.41	22.079 <sup>43</sup>
Sc <sub>2</sub> C	16.31	16.37	16.34	16.40	16.38	16.40	16.31	16.33	16.346 <sup>31</sup>
Y <sub>2</sub> C	18.13	18.16	18.10	18.10	18.19	18.21	18.18	18.20	17.96 <sup>30</sup>
MAE	0.35	0.34	0.39	0.40	0.55	0.59	0.43	0.47	—

Numerical Atomic Orbitals									
Electride	B86bPBE-XDM		PBE-XDM		PBE-MBD-NL		PBE-TS		Experiment
	$c_0$	$c_{\text{th}}$	$c_0$	$c_{\text{th}}$	$c_0$	$c_{\text{th}}$	$c_0$	$c_{\text{th}}$	
Ca <sub>2</sub> N	18.47	18.55	18.54	18.60	18.99	19.04	19.11	19.12	18.114
Sr <sub>2</sub> N	19.91	19.94	19.88	19.93	20.54	20.60	19.97	19.99	19.589
Ba <sub>2</sub> N	20.93	20.98	20.72	20.81	22.00	22.06	21.13	21.16	22.079
Sc <sub>2</sub> C	16.24	16.24	16.33	16.35	16.34	16.36	15.98	16.00	16.346
Y <sub>2</sub> C	17.97	17.98	18.02	18.02	18.16	18.16	17.74	17.76	17.96
MAE	0.39	0.40	0.43	0.43	0.42	0.43	0.58	0.58	—

the  $c$  lattice constant by ca. 1  $\text{\AA}$ . Overall, B86bPBE-XDM/PAW provides the lowest mean absolute errors. PBE-D3 and PBE-D3BJ also provide good performance for the cell volumes, but larger errors in the out-of-plane lattice parameters. The other XDM-corrected functionals and PBE-MBD-NL also perform fairly well on average. Conversely, PBE-TS gives larger errors for both volumes and cell parameters, particularly for the in-plane lattice parameters (see Supplementary Material).

For the best-performing method, B86bPBE-XDM/PAW, full phonon calculations were performed at

each volume to test our use of the Debye model through comparison with the quasi-harmonic approximation (QHA). Table IV shows a comparison of the thermally corrected cell volumes and  $c$  lattice constants obtained with both approximations. Overall, the results are in excellent agreement, validating our use of the Debye model.

Finally, for both the Debye approximation and the QHA, the coefficient of thermal expansion (CTE) was evaluated for each electride and the results are collected in Table IV. There is fairly good agreement between

TABLE IV: Comparison of computed unit-cell volumes ( $V$ ),  $c$ -axis lattice parameters, and coefficients of thermal expansion ( $\alpha$ ), obtained with the Debye and quasi-harmonic approximations, using B86bPBE-XDM/PAW for the standard temperature of 298.15 K. Mean absolute errors (MAEs) are reported for the Debye model relative to the QHA, and for both methods relative to the experimental reference data.

Electride	$V$ ( $\text{\AA}^3$ )		$c$ ( $\text{\AA}$ )		$\alpha$ ( $10^{-5} \text{ K}^{-1}$ )	
	Debye	QHA	Debye	QHA	Debye	QHA
Ca <sub>2</sub> N	204.1	203.4	18.64	18.60	1.9	0.7
Sr <sub>2</sub> N	249.9	248.9	20.14	20.11	2.0	0.7
Ba <sub>2</sub> N	288.9	288.4	21.54	21.52	1.5	0.8
Sc <sub>2</sub> C	155.7	154.0	16.37	16.28	3.0	0.1
Y <sub>2</sub> C	198.5	200.5	18.03	18.11	-2.6	0.3
MAE(QHA)	1.2	-	0.05	-	1.3	-
MAE(Expt.)	7.7	7.4	0.34	0.36	-	-

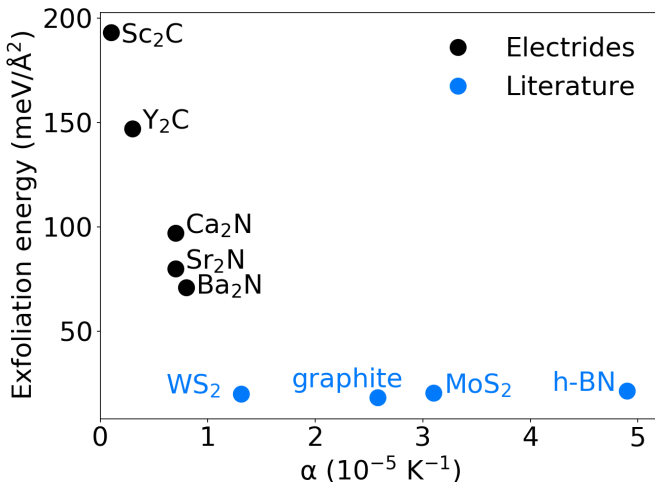


FIG. 3: Plot showing the computed B86bPBE-XDM/PAW exfoliation energies and the QHA thermal expansion coefficients ( $\alpha$ ) for five layered electrides. Data is also shown for four common layered materials characterized in the literature, using a combination of computed exfoliation energies obtained with the same level of theory,<sup>39</sup> together with experimental coefficients of thermal expansion.<sup>74–77</sup>

the Debye and QHA models for the CTEs of the nitride electrides, particularly when considering these values can span orders of magnitude for common materials. However, there is significant disagreement for Y<sub>2</sub>C, where the Debye model predicts thermal contraction and the QHA predicts thermal expansion. As expected based on the small temperature-induced volume changes, the CTEs of all the electrides are very low, particularly with the QHA. Within this approximation, the predicted CTEs are  $0.7 \times 10^{-5} - 0.8 \times 10^{-5} \text{ K}^{-1}$  for the alkaline-earth nitrides, and  $0.1 \times 10^{-5} \text{ K}^{-1}$  and  $0.3 \times 10^{-5} \text{ K}^{-1}$  for the two transition-metal carbides. Figure 3 shows a negative correlation between the CTE and the exfoliation

energy, with the more strongly bound electrides exhibiting the least thermal expansion. Literature CTE values for four common layered materials (graphite,<sup>74</sup> h-BN,<sup>75</sup> MoS<sub>2</sub>,<sup>76</sup> and WS<sub>2</sub><sup>77</sup>), along with computed exfoliation energies,<sup>39</sup> are also plotted for comparison. Overall, relative to these reference materials, the layered electrides have both much stronger exfoliation energies and are predicted to be unusually resistant to thermal expansion. Materials with more comparable CTEs are silicon carbide (a highly rigid material with a diamond crystal structure<sup>78</sup>) and borosilicate glasses, which have values of ca.  $1.0 \times 10^{-5} \text{ K}^{-1}$  at 298.15 K.<sup>79,80</sup>

#### IV. CONCLUSIONS

This work presented a computational study of the thermomechanical properties of five layered electride materials. Calculations employed two electronic structure codes, and six pairs of GGA density functionals and post-self-consistent dispersion corrections. The unit-cell volumes and lattice constants of these materials were evaluated and compared to experimental reference data. The results showed that there are minimal differences between the performance of the various dispersion corrections, with the exception of TS, which gave larger errors, particularly for the cell volumes and in-plane lattice constants. Calculations employing relatively small NAO basis sets provided similar geometries and band structures as plane-wave calculations using the projected augmented-wave method; however, significant differences were found for the exfoliation energies, particularly the absence of a periodic trend for nitride electrides that was present in the PAW data. We conclude that ‘light’ NAO basis sets can be reliably used for geometry optimizations of layered electrides, although subsequent plane-wave calculations would be recommended for single-point energy evaluation and property analysis. NAO calculations are particularly appealing for modeling interfaces (such as in metal-electride-TMDC heterostructures<sup>5</sup>) due to their near-linear scaling with system size.

Additionally, we found that DFT predicts surprisingly low coefficients thermal expansion coefficients for the layered electrides, with values more comparable to those for silicon carbide or borosilicate glasses. Because of this, the inclusion of thermal effects offers no real improvement to the accuracy of the calculated cell volumes and lattice parameters. We conclude that the strong ionic binding, arising from the alternating cationic layers and anionic regions of interstitial electron density, leads to extremely high exfoliation energies and low thermal expansion coefficients for the electrides relative to other classes of layered materials. The low thermal expansion may be an advantage for use of electrides in electronics applications,<sup>5</sup> given the temperature changes that can occur when charge is flowing across an electrical contact.

## SUPPLEMENTARY MATERIAL

Band structures of Sc<sub>2</sub>C and Y<sub>2</sub>C computed using hybrid functionals; band structures of the monolayer electretrenes; static and thermally corrected in-plane lattice parameters; and exfoliation energies, unit-cell volumes, and lattice parameters computed without dispersion corrections. Also available are text files tabulating the electride unit-cell volumes and electronic energies.

## ACKNOWLEDGEMENTS

The authors thank the Natural Sciences and Engineering Council (NSERC) of Canada and the Semiconductor Research Corporation (SRC) for financial support, as well as ACENET and the Digital Research Alliance of Canada for computational resources. We also thank Mohammad Rafiee Diznab for finding the error in the D3 dispersion parameters.

## DATA AVAILABILITY STATEMENT

The data that support this study are provided in this article and its accompanying supplementary material.

## CONFLICTS OF INTEREST

The authors have no conflicts to disclose.

## REFERENCES

- <sup>1</sup>Buchhammagari, H.; Toda, Y.; Hirano, M.; Hosono, H.; Takeuchi, D.; Osakada, K. *Org. Lett.* **2007**, *9*, 4287–4289.
- <sup>2</sup>Choi, S.; Kim, Y. J.; Kim, S. M.; Yang, J. W.; Kim, S. W.; Cho, E. J. *Nat. Commun.* **2014**, *5*, 4881.
- <sup>3</sup>Toda, Y.; Hirayama, H.; Kuganathan, N.; Torrisi, A.; Sushko, P. V.; Hosono, H. *Nat. Commun.* **2013**, *4*, 2378.
- <sup>4</sup>Kitano, M.; Inoue, Y.; Yamazaki, Y.; Hayashi, F.; Kanbara, S.; Matsuishi, S.; Yokoyama, T.; Kim, S.-W.; Hara, M.; Hosono, H. *Nat. Chem.* **2012**, *4*, 934–940.
- <sup>5</sup>Kaadou, F.; Maassen, J.; Johnson, E. R. *J. Phys. Chem. C* **2021**, *125*, 11656–11664.
- <sup>6</sup>Wang, X.; Yu, S.; Xu, Y.; Huang, B.; Dai, Y.; Wei, W. *Phys. Chem. Chem. Phys.* **2023**, *25*, 15433–15440.
- <sup>7</sup>Yanagi, H.; Kim, K.-B.; Koizumi, I.; Kikuchi, M.; Hiramatsu, H.; Miyakawa, M.; Kamiya, T.; Hirano, M.; Hosono, H. *J. Phys. Chem. C* **2009**, *113*, 18379–18384.
- <sup>8</sup>Miyakawa, M.; Kim, S. W.; Hirano, M.; Kohama, Y.; Kawaji, H.; Atake, T.; Ikegami, H.; Kono, K.; Hosono, H. *J. Am. Chem. Soc.* **2007**, *129*, 7270–7271.
- <sup>9</sup>Ellaboudy, A.; Dye, J. L.; Smith, P. B. *J. Am. Chem. Soc.* **1983**, *105*, 6490–6491.
- <sup>10</sup>Dawes, S. B.; Ward, D. L.; Huang, R. H.; Dye, J. L. *J. Am. Chem. Soc.* **1986**, *108*, 3534–3535.
- <sup>11</sup>Huang, R. H.; Wagner, M. J.; Gilbert, D. J.; Reidy-Cedergren, K. A.; Ward, D. L.; Faber, M. K.; Dye, J. L. *J. Am. Chem. Soc.* **1997**, *119*, 3765–3772.
- <sup>12</sup>Redko, M. Y.; Jackson, J. E.; Huang, R. H.; Dye, J. L. *J. Am. Chem. Soc.* **2005**, *127*, 12416–12422.
- <sup>13</sup>Ward, D. L.; Huang, R.; Dye, J. L. *Acta Crystallogr. C Struct. Chem.* **1988**, *44*, 1374–1376.
- <sup>14</sup>Xie, Q.; Huang, R. H.; Ichimura, A. S.; Phillips, R. C.; Pratt Jr, W. P.; Dye, J. L. *J. Am. Chem. Soc.* **2000**, *122*, 6971–6978.
- <sup>15</sup>Matsuishi, S.; Toda, Y.; Miyakawa, M.; Hayashi, K.; Kamiya, T.; Hirano, M.; Tanaka, I.; Hosono, H. *Science* **2003**, *301*, 626–629.
- <sup>16</sup>Hosono, H.; Kitano, M. *Chemical Reviews* **2021**, *121*, 3121–3185.
- <sup>17</sup>Lee, K.; Kim, S. W.; Toda, Y.; Matsuishi, S.; Hosono, H. *Nature* **2013**, *494*, 336–340.
- <sup>18</sup>Druffel, D. L.; Kuntz, K. L.; Woomer, A. H.; Alcorn, F. M.; Hu, J.; Donley, C. L.; Warren, S. C. *J. Am. Chem. Soc.* **2016**, *138*, 16089–16094.
- <sup>19</sup>Zhao, S.; Li, Z.; Yang, J. *J. Am. Chem. Soc.* **2014**, *136*, 1331313318.
- <sup>20</sup>Yi, S.; Choi, J.-H.; Lee, K.; Kim, S. W.; Park, C. H.; Cho, J.-H. *Phys. Rev. B* **2016**, *94*, 235428.
- <sup>21</sup>Druffel, D. L.; Woomer, A. H.; Kuntz, K. L.; Pawlik, J. T.; Warren, S. C. *J. Mater. Chem. C* **2017**, *5*, 11196–11213.
- <sup>22</sup>Dale, S. G.; Johnson, E. R. *Phys. Chem. Chem. Phys.* **2017**, *19*, 27343–27352.
- <sup>23</sup>Zeng, X.; Zhao, S.; Li, Z.; Yang, J. *Phys. Rev. B* **2018**, *98*, 155443.
- <sup>24</sup>Diznab, M. R.; Johnson, E. R.; Maassen, J. *Nanoscale* **2023**,
- <sup>25</sup>Inoshita, T.; Jeong, S.; Hamada, N.; Hosono, H. *Phys. Rev. X* **2014**, *4*, 031023.
- <sup>26</sup>Ming, W.; Yoon, M.; Du, M.-H.; Lee, K.; Kim, S. W. *J. Am. Chem. Soc.* **2016**, *138*, 1533615344.
- <sup>27</sup>Zhang, Y.; Wang, H.; Wang, Y.; Zhang, L.; Ma, Y. *Phys. Rev. X* **2017**, *7*, 011017.
- <sup>28</sup>Zhou, J.; Shen, L.; Yang, M.; Cheng, H.; Kong, W.; Feng, Y. P. *Chem. Mater.* **2019**, *31*, 18601868.
- <sup>29</sup>Walsh, A.; Scanlon, D. O. *J. Mater. Chem. C* **2013**, *1*, 3525–3528.
- <sup>30</sup>Atoji, M.; Kikuchi, M. *J. Chem. Phys.* **1969**, *51*, 3863–3872.
- <sup>31</sup>McRae, L. M.; Radomsky, R. C.; Pawlik, J. T.; Druffel, D. L.; Sundberg, J. D.; Lanetti, M. G.; Donley, C. L.; White, K. L.; Warren, S. C. *J. Am. Chem. Soc.* **2022**, *144*, 10862–10869.
- <sup>32</sup>Mudryk, Y.; Paudyal, D.; Pecharsky, V.; Gschneidner, K. *J. Appl. Phys.* **2011**, *109*.
- <sup>33</sup>Atoji, M. *J. Chem. Phys.* **1969**, *51*, 3872–3876.
- <sup>34</sup>Atoji, M. *J. Chem. Phys.* **1981**, *75*, 1434–1441.
- <sup>35</sup>Atoji, M. *J. Chem. Phys.* **1981**, *74*, 1893–1897.

- <sup>36</sup>McRae, L.; Radomsky, R.; Pawlik, J.; Druffel, D.; Sundberg, J.; Lanetti, M.; Donley, C.; White, K.; Warren, S. **2021**,
- <sup>37</sup>Björkman, T. *J. Chem. Phys.* **2014**, *141*.
- <sup>38</sup>Tawfik, S. A.; Gould, T.; Stampfl, C.; Ford, M. J. *Phys. Rev. Mater.* **2018**, *2*, 034005.
- <sup>39</sup>Otero-de-la-Roza, A.; LeBlanc, L. M.; Johnson, E. R. *J. Phys. Chem. Lett.* **2020**, *11*, 2298–2302.
- <sup>40</sup>Waetzig, K.; Schilm, J. *Int. J. Ceram. Eng. Sci.* **2021**, *3*, 165–172.
- <sup>41</sup>Mackey, J.; Back, T.; Berger, M.-H.; Sayir, A. *J. Am. Ceram. Soc.* **2021**, *104*, 2238–2249.
- <sup>42</sup>Waetzig, K.; Schilm, J.; Drobny, C.; Tajmar, M. *Adv. Eng. Mater.* **2023**, *25*, 2201286.
- <sup>43</sup>Vajenine, G. V.; Grzechnik, A.; Syassen, K.; Loa, I.; Hanfland, M.; Simon, A. *C. R. Chim.* **2005**, *8*, 1897–1905.
- <sup>44</sup>Tkatchenko, A.; Scheffler, M. *Phys. Rev. Lett.* **2009**, *102*, 073005.
- <sup>45</sup>Hermann, J.; Tkatchenko, A. *Phys. Rev. Lett.* **2020**, *124*, 146401.
- <sup>46</sup>Grimme, S.; Antony, J.; Ehrlich, S.; Krieg, H. *J. Chem. Phys.* **2010**, *132*.
- <sup>47</sup>Grimme, S.; Ehrlich, S.; Goerigk, L. *J. Comput. Chem.* **2011**, *32*, 1456–1465.
- <sup>48</sup>Johnson, E. R. In *Non-covalent Interactions in Quantum Chemistry and Physics*; Otero-de-la-Roza, A., DiLabio, G. A., Eds.; Elsevier, 2017; Chapter 5, pp 169–194.
- <sup>49</sup>Otero-de-la-Roza, A.; Johnson, E. R. *J. Chem. Phys.* **2012**, *136*.
- <sup>50</sup>Price, A. J. A.; Otero-de-la-Roza, A.; Johnson, E. R. *Chem. Sci.* **2023**, *14*, 1252–1262.
- <sup>51</sup>Johnson, E. R.; Becke, A. D. *J. Chem. Phys.* **2006**, *124*, 174104.
- <sup>52</sup>Perdew, J. P.; Burke, K.; Ernzerhof, M. *Phys. Rev. Lett.* **1996**, *77*, 3865.
- <sup>53</sup>Becke, A. D. *J. Chem. Phys.* **1986**, *85*, 7184–7187.
- <sup>54</sup>Blum, V.; Gehrke, R.; Hanke, F.; Havu, P.; Havu, V.; Ren, X.; Reuter, K.; Scheffler, M. *Comput. Phys. Commun.* **2009**, *180*, 2175–2196.
- <sup>55</sup>Giannozzi, P. et al. *J. Phys.: Condens. Matter* **2017**, *29*, 465901.
- <sup>56</sup>Johnson, E. R.; Otero-de-la-Roza, A.; Dale, S. G. *J. Chem. Phys.* **2013**, *139*, 184116.
- <sup>57</sup>Janesko, B. G.; Scalmani, G.; Frisch, M. J. *Phys. Chem. Chem. Phys.* **2015**, *17*, 18305–18317.
- <sup>58</sup>Zhang, C.; Bu, Y. *Phys. Chem. Chem. Phys.* **2016**, *18*, 23812–23821.
- <sup>59</sup>Shen, Z.; Peng, S.; Glover, W. J. *J. Chem. Phys.* **2021**, *155*, 224113.
- <sup>60</sup>Dal Corso, A. *Comput. Mater. Sci.* **2014**, *95*, 337–350.
- <sup>61</sup>Methfessel, M.; Paxton, A. *physical review B* **1989**, *40*, 3616.
- <sup>62</sup>Marzari, N.; Vanderbilt, D.; De Vita, A.; Payne, M. *Physical review letters* **1999**, *82*, 3296.
- <sup>63</sup>Price, A. J.; Bryenton, K. R.; Johnson, E. R. *J. Chem. Phys.* **2021**, *154*.
- <sup>64</sup>Otero-de-la-Roza, A.; Abbasi-Pérez, D.; Luaña, V. *Comput. Phys. Commun.* **2011**, *182*, 2232–2248.
- <sup>65</sup>Togo, A.; Tanaka, I. *Scr. Mater.* **2015**, *108*, 1–5.
- <sup>66</sup>Krukau, A. V.; Vydrov, O. A.; Izmaylov, A. F.; Scuseria, G. E. *J. Chem. Phys.* **2006**, *125*.
- <sup>67</sup>Chan, M. K. Y.; Ceder, G. *Phys. Rev. Lett.* **2010**, *105*, 196403.
- <sup>68</sup>Xiao, H.; Tahir-Kheli, J.; III, W. A. G. *J. Phys. Chem. Lett.* **2011**, *2*, 212–217.
- <sup>69</sup>He, J.; Franchini, C. *J. Phys.: Condens. Matter* **2017**, *29*, 454004.
- <sup>70</sup>Adamo, C.; Barone, V. *J. Chem. Phys.* **1999**, *110*, 6158–6170.
- <sup>71</sup>Spanu, L.; Sorella, S.; Galli, G. *Phys. Rev. Lett.* **2009**, *103*, 196401.
- <sup>72</sup>Fang, Z.; Li, X.; Shi, W.; Li, Z.; Guo, Y.; Chen, Q.; Peng, L.; Wei, X. *The J. Phys. Chem. C* **2020**, *124*, 23419–23425.
- <sup>73</sup>Adeleke, A. A.; Johnson, E. R. *Phys. Rev. B* **2023**, *107*, 064101.
- <sup>74</sup>Fried, L. E.; Howard, W. M. *Phys. Rev. B* **2000**, *61*, 8734.
- <sup>75</sup>Zhao, Y.; Von Dreele, R. B.; Weidner, D. J.; Schiferl, D. *Int. J. High Press. Res.* **1997**, *15*, 369–386.
- <sup>76</sup>Fan, D.; Xu, J.; Ma, M.; Liu, J.; Xie, H. *Phys. B: Condens.* **2014**, *451*, 53–57.
- <sup>77</sup>Vasiliev, O. *Powder Metallurgy and Metal Ceramics* **2021**, *59*, 576–584.
- <sup>78</sup>Taylor, A.; Laidler, D. *Br. J. Appl. Phys.* **1950**, *1*, 174.
- <sup>79</sup>Wang, Y.; Liu, Z. T.; Khare, S. V.; Collins, S. A.; Zhang, J.; Wang, L.; Zhao, Y. *Appl. Phys. Lett.* **2016**, *108*.
- <sup>80</sup><https://www.schott.com/en-my/products/mempax-p1000322/technical-details>.